ACS Applied Materials & Interfaces, 2014, Volume 6, Issue 14, Pages 11633–11639

Energy-storage properties and electrocaloric effect of $Pb_{(1-3x/2)}La_xZr_{0.85}Ti_{0.15}O_3$ antiferroelectric thick films

Ye Zhao[1], Xihong Hao[1,*], and Qi Zhang[2,3]

1-School of Materials and Metallurgy, Inner Mongolia University of Science and Technology, Baotou 014010, China

2-State Key Laboratory of Advanced Technology for Materials Synthesis and Processing, Wuhan University of Technology, Wuhan 430070, Hubei, China

3-Department of Manufacturing and Materials, Cranfield University, Cranfield, Bedfordshire, MK43 0AL, UK

Abstract: 1-μm-$Pb_{(1-3x/2)}La_xZr_{0.85}Ti_{0.15}O_3$ (PLZT) antiferroelectric (AFE) thick films with x = 0.08, 0.10, 0.12, and 0.14 were deposited on $LaNiO_3$/Si (100) substrates by a sol-gel method. The dielectric properties, energy-storage performance, electrocaloric effect, and leakage current behavior were investigated in detail. With increasing La content, dielectric constant and saturated polarizations of the thick films were gradually decreased. A maximum recoverable energy-storage density of 38 J/cm^3 and efficiency of 71% were achieved in the thick films with x = 0.12 at room temperature. Moreover, a large reversible adiabatic temperature change ΔT = 25.0 ^{o}C was presented in the thick films with x = 0.08 at 127 ^{o}C at 990 kV/cm. All the samples had a lower leakage current density below 10^{-6} A/cm^2 at room temperature. These results indicated that the PLZT AFE thick films could be a potential candidate for applications in high energy-storage density capacitors and cooling devices.

Keyword: PLZT thick films; sol-gel; dielectric properties; energy-storage properties; electrocaloric effect

*Corresponding author: xhhao@imust.cn; Tel: +86-472-5951572; Fax: +86-472-5951571

1. Introduction

Lead zirconate ($PbZrO_3$) was the first compound identified as an antiferroelectric (AFE) in 1951 [1]. Under sufficiently high external electric filed, a ferroelectric state can be induced in AFEs and this transition is often accompanied by larger strains and polarization changes [2-3]. Therefore, Pb-based AFE materials have attracted increasing attention for the potential applications in high energy storage capacitors, micro-actuators, pyroelectric security sensors, cooling devices, and pulsed power generators and so on [4-8].

Up to now, the reported works on energy-storage properties and electrocaloric effect (ECE) of AFE materials mainly focused on bulk ceramics and thin films [9-12]. Because of the lower breakdown strength (BDS), the energy-storage density and ECE of the bulk ceramics are usually very small. For example, it was reported that the maximum energy-storage density and ECE obtained in the AFE bulk ceramics are only 2.75 J/cm^3 and 2.5 K, respectively [13, 14]. It was recognized that the lower BDS was one of the main reasons for the small energy-storage density and weak ECE, which hindered the AFE bulk ceramics for practical applications. Thus, it was predicated that an improved energy-storage performance and ECE could be realized in AFE thin films, because of their good electric-field endurance. For instance, a large energy-storage density of 14.9 J/cm^3 and 14.6 J/cm^3 were reported in La and Sr-doped $PbZrO_3$ AFE thin films by Parui and Hao, respectively [15, 16]. Similarly, a giant ECE of 12 K at 25 V was obtained in 350-nm-thick $PbZr_{0.95}Ti_{0.05}O_3$ AFE films near its Curie temperature by Mischenko *et.al.* [17]. Very recently, a much larger ECE of 45.3 K at room temperature was reported in 320-nm-thick $Pb_{0.8}Ba_{0.2}ZrO_3$ films [18]. These results raised hopes for the realization of ECE-based solid-state cooling devices. However, because of their small

thickness (<1μm), the overall stored energy and heat-sinking capacity of the AFE thin films are still not so high as to satisfy the requirement of practical applications. As a result, it could be concluded that, due to the higher BDS and larger overall volume, thick films (1-100 μm) might overcome the shortcomings of bulk ceramics and thin films and are suitable for the applications in high energy-storage and cooling devices.

Unfortunately, the energy-storage properties and ECE in AFE thick films were rarely studied, especially on their cooling characteristics. Thus, in this work, 1-μm-$Pb_{(1-3x/2)}La_x(Zr_{0.85}Ti_{0.15})O_3$ system AFE thick films were fabricated via a sol-gel technique. The aim of this work is to examine the energy-storage properties and ECE of PLZT AFE thick films.

2. Experimental procedure

$Pb_{1-3x/2}La_xZr_{0.85}Ti_{0.15}O_3$ (PLZT) AFE thick films with x = 0.08, 0.10, 0.12, and 0.14 were grown on $LaNiO_3$/Si (100) substrates by using a sol-gel method. Lead acetate trihydrate, lanthanum acetate, titanium isopropoxide, and zirconium isopropoxide were used as the raw materials. Glacial acetic and deionized water were used as solvents. Lactic acid functioned as catalyzer and chelation agent was added into the solution in the ratio of one mole of lactic acid to one mole of lead. In order to improve the mechanical properties of the gel film, ethylene glycol was also added into the solution in the ratio of one mole of ethylene glycol to one mole of lead. 20 mol% excess of lead acetate trihydrate was introduced to compensate the lead loss during annealing and to prevent the formation of pyrochlore phase in the films. The concentration of the precursor solution was 0.5 M. The conductive $LaNiO_3$ (LNO) films with a thickness of about 250 nm were chosen as bottom electrodes, which were prepared on Si (100) substrates by the chemical solution deposition route and was similar

to Ref. 19. The obtained LNO films showed a (100) growth orientation.

After aged for 24 h, PLZT AFE films were deposited on LNO/Si (100) substrates through a multiple-step spin-coating technique. Each PLZT AFE film was spin coated at 3000 rpm for 40 s. In order to reduce the formation of cracks, every wet film was first dried at 350 ^{o}C for 10 min and subsequently pyrolyzed at 600 ^{o}C for 10 min. The spin-coating and heat-treatment were repeated several times to obtain the desired thickness. To prevent excessive lead loss and form pure perovskite phase, a capping layer of 0.4 M PbO precursor solution which was prepared from lead acetate trihydrate was added before the films went through a final anneal at 700 ^{o}C for 30 min. The final thickness of all the PLZT AFE thick films was about 1 μm, which was determined by the crossing-section FE-SEM picture.

The microstructure of all the PLZT AFE thick films was analyzed by X-ray diffraction (XRD Bruker D8 Advanced Diffractometer, German) and field-emission scanning electron microscopy (FE-SEM ZEISS Supra 55, German), respectively. For the measurements of electrical properties, gold pads of 0.2 mm in diameter were coated on the surface as top electrodes by using a dc sputtering method. The frequency and temperature-dependent dielectric properties of the PLZT AFE thick films were measured by using a computer-controlled Agilent E4980A LCR analyzer. The polarization-electric field hysteresis loops (*P-E*) and the leakage current characteristic of the PLZT AFE thick films were measured by a Radiant Technology Ferroelectric tester with high-voltage power supply (Trek Inc., Media, NY). The energy-storage performance and ECE were calculated according to the *P-E* results. For convenience, the samples of x = 0.08, 0.10, 0.12, and 0.14 were abbreviated as PLZT8/85/15, PLZT 10/85/15, PLZT 12/85/15, and PLZT 14/85/15, respectively.

3. Results and discussion

Fig. 1 shows the XRD patterns of the PLZT AFE thick films with different x values after being annealed at 700 ^{o}C. All the thick films exhibit good crystalline quality and a pure polycrystalline perovskite phase with orthorhombic structure. For convenience, the lattice indexes of the peaks were labeled as pseudocubic structure, according to the results reported by Hao *et.al.* [16]. Moreover, it could be found from the curves that all the PLZT AFE thick films showed (100)-preferred orientation, which was attributed to the same grown orientation of LNO bottom electrodes.

The surface FE-SEM morphology images of the thick films with different x values are shown in Fig. 2(a)-2(d). It is noted that the surface microstructures of the obtained films have a close relation with the La content. Evidently, with the La content increasing, the grain size of the samples changes significantly. All the samples exhibit dense and void-free structure, which was ascribed to the two-step heat-treatment technique during the fabrication process. The insets of Fig. 2(a)-2(d) present the corresponding cross-section images of the films. It can be seen that the all films ~~shared the similar~~ show a thickness of about 1 μm. In addition, the microscopic results further demonstrated that all the films possessed a uniform and dense microstructure.

Frequency-dependent dielectric constant and dielectric loss of these thick films are plotted in Fig. 3, which were measured from 1 kHz to 1 MHz at room temperature. As the frequency increases, the dielectric constant for all the samples gradually decreases. The declined tendency was caused by the long-time polarization process of some frameworks, such as space charges, which had no contribution to the overall polarization at higher frequency. Moreover, the composition of the films had a clear effect on their dielectric constant. As x increases from 0.08 to 0.14, the dielectric constant

decreases. For example, dielectric constant at 1 MHz was 862, 618, 433, and 358 for x = 0.08, 0.10, 0.12, and 0.14, respectively. However, the dielectric loss of these thick films was slightly composition-dependent, and all the films share the similar values in dielectric loss. With the measurement frequency increasing, the dielectric loss increases, which was caused by the polarization relaxor.

Electric-field-dependent dielectric constants (ε_r-E) of the PLZT AFE thick films with different x values are plotted in Fig. 4, which were measured at room temperature and at 100 kHz. The dc field was stepped at a time lag of 0.5 s according to the following measurement mode: zero to E_{max}, E_{max} to - E_{max}, and - E_{max} to zero. All the ε_r-E curves show double butterfly behavior, corresponding to the transformation between AFE to FE phases. The dielectric constant sharply increases at the moment of the AFE-FE transition and then drops when the curve saturated. The phase switching field can be determined from peaks of the ε_r-E curves. The phase transformation fields of the PLZT AFE thick films are shown in the inset of Fig. 4. Clearly, the forward phase switching (AFE-to-FE) fields (E_F) are approximately 136 kV/cm, 155 kV/cm, 175 kV/cm, 175 kV/cm and the reverse backward phase switching (FE-to-AFE) fields (E_A) are approximately 70 kV/cm, 110 kV/cm, 130 kV/cm, 130 kV/cm for the thick films with x = 0.08, 0.10, 0.12, and 0.14, respectively. Namely, with La content increasing, the phase switching fields increase. Similar results were also reported in La-doped bulk AFE ceramics [20]. The possible reason could be given according to the tolerance factor t [21], which was defined as:

$$t = \frac{r_A + r_O}{\sqrt{2}(r_B + r_O)}, \quad (1)$$

where r_A, r_B, and r_O were the ionic radii of A-site cation, B-site cation, and oxygen anion,

respectively. It was generally believed that FE phase was stabilized for t>1 and that AFE phase was stabilized for t<1 [22]. According to the formula, *t* value decreases with the La adding, because the ionic radii (0.149 nm) of Pb^{2+} was larger than that (0.136 nm) of La^{3+}. This result indicates that the addition of La is favor to stabilize the AFE state.

Fig. 5(a) shows the temperature dependence of dielectric constant for PLZT AFE thick films, which were measured at 100 kHz. Obviously, all the curves exhibit a typical diffused phase transition from AFE to paraelectric (PE) phase, indicating good temperature stability of dielectric properties. Moreover, the temperature (T_m) corresponding to the maximum dielectric constant is shifted to low temperature with the La content increasing. The values of T_m are presented in the inset of Fig. 5 (a), which is 170 °C, 134 °C, 130 °C, and 95 °C for the samples with x = 0.08, 0.10, 0.12, and 0.14, respectively. This result is consistent to the results of Xu *al.et.* in $(Pb,La)(Zr_{0.85}Ti_{0.15})O_3$ ceramics [20]. The dielectric constant of the PLZT AFE thick films with x = 0.08 as a function of dc field and temperature at 100 kHz are plotted in Fig. 5(b). With a zero field, a transition between the AFE phase and a PE phase occurred at 170 °C. With the dc field increasing, the dielectric peak of the films moved to lower temperature, which is similar with the report of Zhang *et.al.* in lead zirconate stannate titanate based AFE bulk ceramics [23].

Room temperature polarization-electric field hysteresis loops of the PLZT AFE thick films with different x values are shown in Fig. 6, which were measured at 1 kHz and at 600 kV/cm. All the samples exhibit a slim and double *P-E* loops, indicating their AFE nature. Moreover, the saturated polarizations (P_s) and the remnant polarization (P_r) decrease substantially with La content increasing. For example, P_s and P_r are 62, 49, 41, 39 μC/cm^2 and 10, 5, 4, 4 μC/cm^2 for the films with x = 0.08,

0.10, 0.12, and 0.14, respectively. This result is consistent to the results of Es-Souni *al.et.* in $Pb_{1-x}La_x(Zr_{0.52}Ti_{0.48})_{1-x/4}O_3$ thin films [24]. The inset of Fig. 6 gives the *P-E* loops at their critical breakdown strength. Clearly, large differences between P_s and P_r were realized at their BDS, indicating that a high recyclable energy-storage density could be obtained in these films.

Fig. 7(a) illustrates the electric field dependence of recyclable energy-storage density and energy-storage efficiency of the PLZT AFE thick films with different x values, which were measured from 200 kV/cm to their BDS at 1 kHz and at room temperature. Commonly, the recoverable energy-storage density *W* could be estimated from the *P-E* loops, which is calculated with the equation as below:

$$W = \int_{P_r}^{P_{max}} EdP, \tag{2}$$

where *E* is the applied electric field, *P* is the polarization and P_{max} is the maximum polarization. According to equation (2), materials with smaller P_r, larger P_{max} and higher BDS are more suitable for energy storage. Clearly, the *W* values of all the samples gradually increase as the electric field is increased. The *W* values at their corresponding BDS were 33, 35, 38, and 29 J/cm^3 for the PLZT AFE thick films with x = 0.08, 0.10, 0.12, and 0.14, respectively. Moreover, in the measurement range, the *W* values for PLZT AFE thick films with x = 0.12 were comparatively higher than other samples. In practical application, apart from higher recyclable energy-storage density *W* values, larger energy-storage efficiency η is also always desired. The energy-storage efficiency η is calculated as the following formula:

$$\eta = \frac{W}{W + W_{loss}}, \tag{3}$$

where W_{loss} is the energy loss density, calculated by the numerical integration of closed area of the hysteresis loops. Obviously, different from the *W* values, the η values of PLZT AFE thick films

decrease gradually with the increasing of the measured electric field. For example, the η value of PLZT AFE thick films with x = 0.12 gradually decreases from 85% to 71%. The inset in Fig. 7(a) depicts Weibull distribution of BDS for the PLZT AFE thick films. The relevant detailed description on Weibull distribution could be found in Ref. 25. According to the data given in the inset, the BDS values of the films with x = 0.08, 0.10, 0.12, and 0.14 obtained from the X intercept of the fitting lines were 1820, 2112, 2141, and 1827 kV/cm, respectively. The high BDS of samples were attributed to their denser microstructure. It is well known that the temperature-dependent stability of the energy-storage performance is also an important parameter in practical application. Fig. 7(b) shows the energy-storage performance of all the PLZT AFE thick films in the temperature range of 20-150 ^{o}C, which were measured at 1 kHz and at 900 kV/cm. Clearly, all the curves were only slightly fluctuated in the measurement range, indicating good temperature stability of the energy-storage performance.

Fig. 8 shows the adiabatic temperature change ΔT of the PLZT AFE thick films with x = 0.08 under different electric field changes ΔE. Reversible adiabatic changes in temperature ΔT for a material of density ρ with heat capacity C are expressed [14] by:

$$\Delta T = -\frac{1}{C\rho}\int_{E_1}^{E_2} T\left(\frac{\partial P}{\partial T}\right)_E dE, \tag{4}$$

assuming the Maxwell relation $\left(\frac{\partial P}{\partial T}\right)_E = \left(\frac{\partial S}{\partial E}\right)_T$. Values of $\left(\frac{\partial P}{\partial T}\right)_E$ were obtained from fourth-order polynomial fits to raw $P(T)$ data extracted from the upper branches of P-E loops in $E > 0$, as shown in inset of Fig. 8. In the temperature range of interest the heat capacity C = 330 J•K^{-1}•kg^{-1} remains constant for Zr-rich lead-based films and the peak associated with the transition is < 10% of the background [17]. The theoretical density ρ of the PLZT AFE thick films are calculated from the

convention of orthorhombic cell parameters. The orthorhombic cell parameters of the PLZT are calculated from the relationship as following [25]:

$$d_{hkl} = \frac{1}{\sqrt{\left(\frac{h}{a}\right)^2 + \left(\frac{k}{b}\right)^2 + \left(\frac{l}{c}\right)^2}}, \quad (5)$$

where d_{hkl} is the interplanar spacing, which are obtained from the XRD patterns. Thus, the calculated ρ values are about 7.9 g•cm^{-3} for all the samples. Here $E_1 = 0$ and $E_2 = E$, thus ΔE is equal to E. Clearly, the obvious temperature changes are obtained below the AFE-PE phase transformation, and the maximum value of ΔT increases with the applied electric field increasing. The maximum ΔT (= 25 ^{o}C) of the thick films with x = 0.08 at 127 ^{o}C was received at 990 kV/cm. The value of the maximum ΔT in this film is higher than that (ΔT = 8.5 at 220 ^{o}C) obtained in $Pb_{0.97}La_{0.02}(Zr_{0.95}Ti_{0.05})O_3$ thick films [8].

Fig. 9 shows the adiabatic temperature change ΔT of the PLZT AFE thick films with different x values under ΔE = 990 kV/cm. Clearly, the peaks of ΔT are shifted to low temperature with the La content increasing. For example, the temperature corresponding to the peak of ΔT of the thick films with x = 0.08, 0.10, 0.12, and 0.14 are 127, 114, 87, and 54 ^{o}C at 990 kV/cm, respectively. Evidently, the peak of ΔT could also be adjusted by the content of La. Under the measurement condition, the peak value of ΔT for the AFE films with x = 0.08, 0.10, 0.12, and 0.14 are 25.0, 10.2, 7.2, and 10.4 ^{o}C, respectively. Moreover, it can be found from these figures that all the curves display diffused character, indicating that these films are able to operate in a wide temperature range. Generally, the peak of ΔT is usually located near T_m, and was moved to higher temperature with the increase of applied electric field. However, in the present work, the temperatures corresponding to the peak of ΔT are lower than their T_m. The possible reason may be contributed to the declined phase transition temperature between AFE to PE state under the function of external electric field, as shown in Fig.

5(b).

Fig. 10 shows the electrocaloric coefficient (ξ_{max}) and refrigeration efficiency (*COP*) of all the PLZT AFE thick films at 990 kV/cm. Electrocaloric coefficient is defined as $\xi_{max} = \Delta T_{max}/\Delta E_{max}$, where ΔT_{max} is the maximum temperature change, and ΔE_{max} is the corresponding electric field change. Clearly, the ξ_{max} of the thick films with x = 0.08, 0.10, 0.12, and 0.14 are 0.025, 0.007, 0.010, and 0.011 K•cm/kV respectively. A maximum electrocaloric coefficient of 0.025 K•cm/kV is achieved in the films with x = 0.08, which is higher than other lead-based films, such as $0.9PbMg_{1/3}Nb_{2/3}O_3$-$0.1PbTiO_3$ (ξ_{max} = 0.006 K•cm/kV) and $PbSc_{0.5}Ta_{0.5}O_3$ (ξ_{max} = 0.008 K•cm/kV) [11, 26]. In order to give a comparison criterion for electrocaloric refrigeration, Emmanuel *et.al.* introduced the refrigeration efficiency, which is given as [27]:

$$COP = \frac{|Q|}{|W|} = \frac{|\Delta S \times T|}{|W|}, \tag{6}$$

$$\Delta S = -\int_{E_1}^{E_2} \left(\frac{\partial P}{\partial T}\right)_E dE, \tag{7}$$

where Q is isothermal heat and ΔS is entropy. Based on above formulas, the calculated *COP* values of the thick films with x = 0.08, 0.10, 0.12, and 0.14 are 4.4, 1.3, 1.5, and 1.7 at 990 kV/cm, respectively. The maximum *COP* is found to be 4.4 of the thick films with x = 0.08, which is higher than 3.0 obtained in $PbZr_{0.95}Ti_{0.05}O_3$ [27].

Fig. 11(a) shows the time relaxation for the current density of these PLZT AFE thick films, which were measured at room temperature and at 400 kV/cm. Clearly, the leakage current density shows strong initial-time dependence because of the dielectric polarization relaxation, which obeys the Curie-von Schweidler law as follows [28]:

$$J = J_s + J_0 \times t^{-n}, \tag{8}$$

where J_s is the steady-state current density, J_0 is a fitting constant, t is the relaxation time in second,

and n is the slope of the log-log plot. There possible mechanisms are associated with the Curie-von Schweidler law: space charge trapping, relaxation time distribution and electrical charge hopping [29]. Fitting the date to Eq. (8), the steady-state current densities for the films with x = 0.08, 0.10, 0.12, and 0.14 are 1.30×10^{-6}, 1.13×10^{-6}, 9.23×10^{-7}, and 7.49×10^{-7} A/cm^2, respectively. It could be learned from these results that all films had a small J_s in the given operation condition and the leakage current densities decreased with increasing x values. The corresponding La content dependences of steady-state leakage current are given in the inset of Fig. 11(a), which was 0.69, 0.53, 0.43, and 0.40 nA for the films with x = 0.08, 0.10, 0.12, and 0.14 , respectively. The smaller leakage currents yielded negligible Joule heating (~ 10^{-4} K) and did not affect P-E results because currents of hundreds of μA were required to switch the measured polarizations at 1 kHz. Fig. 11(b) presents the current density-time characteristics of the thick films with x = 0.14 measured at the temperature range of 20-150 ^{o}C and at 400 kV/cm. Clearly, the leakage current density of the sample increases with increasing temperature. The values of J_s are shown in the inset of Fig.11(b). The steady-state current density at 400 kV/cm is 8.48×10^{-7}, 3.71×10^{-6}, 1.28×10^{-6}, and 4.78×10^{-5} A/cm^2 for the sample at 20 ^{o}C, 50 ^{o}C, 100 ^{o}C, and 150 ^{o}C, respectively. This result indicated that the films possess a good dielectric property even at higher temperature, which was favor to their application in cooling devices.

4. Conclusion

In conclusion, (100)-preferred $Pb_{(1-3x/2)}La_xZr_{0.85}Ti_{0.15}O_3$ (x = 0.08-0.14)AFE thick films with a thickness of 1 μm were successfully fabricated by using a sol-gel method. It is found that the dielectric properties of the films were strongly dependent on the content of La. As a result, the

energy-storage properties and ECE were also tuned accordingly. A maximum recoverable energy-storage density of 38 J/cm^3 at room temperature were achieved in the films with x = 0.12. Moreover, all the samples showed good energy-storage stability in the temperature range of from 20 ^{o}C to 150 ^{o}C. A large reversible adiabatic temperature change (ΔT = 25.0 ^{o}C) at 127 ^{o}C was obtained in the film with x = 0.08, at the same time, large electrocaloric coefficient of 0.025 K•cm/kV and refrigeration efficiency of 4.4 were also realized in this films. These properties indicate that the PLZT AFE thick films have strong potential application in energy-storage and cooling devices.

Acknowledgments

The authors would like to acknowledge the financial support from the National Natural Science Foundation of China under grant no. 51002071, the Program for New Century Excellent Talents in University (2012), the Program for Young Talents of Science and Technology in Universities of Inner Mongolia Autonomous Region.

Reference

[1] Shirane, G.; Sawaguchi, E.; Takagi, Y. Dielectric Properties of Lead Zirconate. *Phys. Rev.* **1951**, *84*, 476-481.

[2] Mirshekarloo, M. S.; Yao, K.; Sritharan, T. Large Strain and High Energy Storage Density in Orthorhombic Perovskite $(Pb_{0.97}La_{0.02})(Zr_{1-x-y}Sn_xTi_y)O_3$ Antiferroelectric Thin Films. *Appl. Phys. Lett.* **2010**, *97*, 142902.

[3] Hao, X.; Zhai, J.; Yang, J.; Ren, H.; Song, X. Improved Field-induced Strains and Fatigue Endurance of PLZT Antiferroelectric Thick Films by Orientation Control. *Phys. Status Solidi RRL* **2009**, *3*, 248-250.

[4] Hao, X.; Zhai, J.; Kong, L. B.; Xu, Z. A. Comprehensive Review on the Progress of Lead Zirconate-based Antiferroelectric Materials. *Prog. Mater. Sci.* **2014**, *63*, 1-57.

[5] Xu, Z.; Zhai, J.; Chan, W. H.; Chen, H. Phase Transformation and Electric Field Tunable Pyroelectric Behavior of $Pb(Nb,Zr,Sn,Ti)O_3$ and $(Pb,La)(Zr,Sn,Ti)O_3$ Antiferroelectric Thin Films. *Appl. Phys. Lett.* **2006**, *88*, 132908.

[6] Wang, Y.; Hao, X.; Xu, J. Effects of PbO Insert Layer on the Microstructure and Energy Storage Performances of (042)-preferred PLZT Antiferroelectric Thick Films. *J. Mater. Res.* **2012**, *27*, 1770-1775.

[7] Tong, S.; Ma, B.; Narayanan, M.; Liu, S.; Koritala, R.; Balachandran, U.; Shi, D. Lead Lanthanum Zirconate Titanate Ceramic Thin Films for Energy Storage. *ACS Appl. Mater. Interfaces* **2013**, *5*, 1474-1480.

[8] Hao, X.; Yue, Z.; Xu, J.; An, S.; Nan, C. W. Energy-storage Performance and Electrocaloric Effect in (100)-oriented $Pb_{0.97}La_{0.02}(Zr_{0.95}Ti0._{05})O_3$ Antiferroelectric Thick Films. *J. Appl. Phys.* **2011**, *110*, 064109.

[9] Ge, J.; Dong, X.; Chen, Y.; Cao, F.; Wang, G. Enhanced Polarization Switching and Energy-storage Properties of $Pb_{0.97}La_{0.02}(Zr_{0.95}Ti_{0.05})O_3$ Antiferroelectric Thin Films with $LaNiO_3$ Oxide Top Electrodes. *Appl. Phys. Lett.* **2013**, *102*, 142905.

[10] Wang, B.; Luo, L.; Jiang, X.; Li, W.; Chen, H. Energy-storage Properties of (1-x)$Bi_{0.47}Na_{0.47}Ba_{0.06}TiO_3$-x$KNbO_3$ Lead-free Ceramics. *J. Alloys Compd.* **2014**, *585*, 14-18.

[11] Mischenko, A. S.; Zhang, Q.; Whatmore, R. W.; Mathur, N. D. Giant Electrocaloric Effect in the Thin Film Relaxor Ferroelectric 0.9$PbMg_{1/3}Nb_{2/3}O_3$-0.1$PbTiO_3$ Near Room Temperature. *Appl. Phys. Lett.* **2006**, *89*, 242912.

[12] Xiao, D. Q.; Wang, Y. C.; Zhang, R. L.; Peng, S. Q.; Zhu, J. G.; Yang, B. Electrocaloric Properties of (1-x)$Pb(Mg_{1/3}Nb_{2/3})O_3$-x$PbTiO_3$ Ferroelectric Ceramics Near Room Temperature. *Mater. Chem. Phys.* **1998**, *57*, 182-185.

[13] Zhang, L.; Jiang, S.; Zeng, Y.; Fu, M.; Han, K.; Li, Q.; Wang, Q.; Zhang, G. Y Doping and Grain Size Co-effects on the Electrical Energy Storage Performance of $(Pb_{0.87}Ba_{0.1}La_{0.02})(Zr_{0.65}Sn_{0.3}Ti_{0.05})O_3$ Anti-ferroelectric Ceramics. *Ceram. Int.* **2014**, *40*, 5455-5460.

[14] Tuttle, B. A.; Payne, D. A. The Effects of Microstructure on the Electrocaloric Properties of $Pb(Zr,Sn,Ti)O_3$ Ceramics. *Ferroelectrics* **1981**, *37*, 603-606.

[15] Parui, J.; Krupanidhi, S. B. Enhancement of Charge and Energy Storage in Sol-gel Derived Pure and La-modified $PbZrO_3$ Thin Films. *Appl. Phys. Lett.* **2008**, *92*, 192901.

[16] Hao, X.; Zhai, J.; Yao, X. Improved Energy Storage Performance and Fatigue Endurance of Sr-doped $PbZrO_3$ Antiferroelectric Thin Films, *J. Am. Cram. Soc.* **2009**, *92*, 1133-1135.

[17] Mischenko, A. S.; Zhang, Q.; Scott, J. F.; Whatmore，R. W.; Mathur, N. D. Giant Electrocaloric Effect in Thin-Film $PbZr_{0.95}Ti_{0.05}O_3$. *Science* **2006**, *311*, 1270-1271.

[18] Peng, B.; Fan, H.; Zhang, Q. A Giant Eletrocaloric Effect in Nanoscale Antiferroelectric and Ferroelectric Phases Coexisting in a Relaxor $Pb_{0.8}Ba_{0.2}ZrO_3$ Thin Film at Room Temperature. *Adv. Funct. Mater.* **2013**, *23*, 2987-2992.

[19] Meng, X. J.; Sun, J. L.; Yu, J.; Ye, H. J.; Guo, S. L.; Chu, J. H. Preparation of Highly (100)-oriented Metallic $LaNiO_3$ Films on Si Substrates by a Modifed Metalorganic Decomposition Technique. *Appl. Surf. Sci.* **2001**, *171*, 68-70.

[20] Xu, Z.; Dai, X.; Li, J.; Viehland, D. Coexistence of Incommensurate Antiferroelectric and Relaxorlike Ferroelectric Orderings in High Zrcontent Lamodified Lead Zirconate Titanate Ceramics. *Appl. Phys. Lett.* **1996**, *68*, 1628-1630.

[21] Hao, X.; Wang, Y.; Zhang, L.; Zhang, L.; An, S. Composition-dependent Dielectric and Energy-storage Properties of (Pb,La)(Zr,Sn,Ti)O_3 Antiferroelectric Thick Films. *Appl. Phys. Lett.* **2013**, *102*, 163903.

[22] Pan, M. J.; Park, S. E.; Markowski, K. A.; Hackenberger, W. S.; Yoshikawa, S.; Cross, L. E. Electric Field Induced Phase Transition in Lead Lanthanum Stannate Zirconate Titanate (PLSnZT) Antiferroelectrics: Tailoring Properties Through Compositional Modification. *Ferroelectrics* **1998**, *215*, 153-167.

[23] Zhang, Q.; Chen, S.; Fan, M.; Jiang, S.; yang, T.; Wang, J.; Li, G.; Yao, X. High Pyroelectric Response of Lead Zirconate Stannate Titanate Based Antiferroelectric Ceramics with Low Curie Temperature. *Mater. Res. Bull.* **2012**, *47*, 4503-4509.

[24] Es-Souni, M.; Abed, M.; Piorra, A.; Malinowski, S.; Zaporojtchenko, V. Microstructure and Properties of Sol-gel Processed $Pb_{1-x}La_x(Zr_{0.52}, Ti_{0.48})_{1-x/4}O_3$ Thin Films. The Effects of Lanthanum Content and Bottom Electrodes. *Thin Solid Films* **2001**, *389*, 99-107.

[25] Zhao, Y.; Hao, X.; Li, M. Dielectric Properties and Energy-storage Performance of $(Na_{0.5}Bi_{0.5})TiO_3$ Thick Films. *J. Alloys Comp.* **2014**, *601*, 112-115.

[26] Lakhdar, M. H.; Ouni, B.; Amlouk, M. Thickness Effect on the Structural and Optical Constants of Stibnite Thin Films Prepared by Sulfidation Annealing of Antimony Films. *Optik-Int. J. Light Electron Opt.* **2014**, DOI.org/10.1016/j.ijleo.2013.10.114.

[27] Correia, T. M.; Kar-Narayan, S.; Young, J. S.; Scott, J. F.; Mathur, N. D.; Whatmore, R. W.; Zhang, Q. PST Thin Films for Electrocaloric Coolers. *J. Phys. D: Appl. Phys.* **2011**, *44*, 165407.

[28] Defay, E.; Crossley, S.; Kar-Narayan, S.; Moya, X.; Mathur, N. D. The Electrocaloric Efficiency of Ceramic and Polymer Films. *Adv. Mater.* **201**3, *25*, 3337-3342.

[29] Ma, B.; Kwon, D. K.; Narayanan, M.; Balachandran, U. B. Leakage Current Characteristics and Dielectric Breakdown of Antiferroelectric $Pb_{0.92}La_{0.08}Zr_{0.95}Ti_{0.05}O_3$ Film Capacitors Grown on Metal Foils. *J. Phys. D: Appl. Phys.* **2008**, *41*, 205003.

[30] Zhang, L.; Hao, X. Dielectric Properties and Energy-storage Performances of $(1-x)(Na_{0.5}Bi_{0.5})TiO_3$-$xSrTiO_3$ Thick Films Prepared by Screen Printing Technique. *J. Alloys Comp.* **2014**, *586*, 674-678.

Figure caption

Fig. 1 XRD patterns of the PLZT AFE thick films with x = 0.08, 0.10, 0.12, and 0.14.

Fig. 2 Surface FE-SEM morphology images of the PLZT AFE thick films with x = 0.08, 0.10, 0.12, and 0.14. The inset is the corresponding cross-section images of the films.

Fig. 3 Room temperature frequency-dependent dielectric constant and dielectric loss of the PLZT AFE thick films with x = 0.08, 0.10, 0.12, and 0.14.

Fig. 4 Dielectric constant as a function of dc voltage at 100 kHz of the PLZT AFE thick films with x = 0.08, 0.10, 0.12, and 0.14.

Fig. 5 (a) Temperature dependence of dielectric constant of PLZT AFE thick films with x = 0.08, 0.10, 0.12, and 0.14. The inset is the maximum permittivity temperature of these films. (b) Temperature dependence of dielectric constant of PLZT AFE thick films with x = 0.08 at 100 kHz under various dc electric fields.

Fig. 6 Room temperature *P-E* loops of the PLZT AFE thick films with x = 0.08, 0.10, 0.12, and 0.14 at 600 kV/cm and at 1 kHz. The inset is the *P-E* loops at their critical breakdown strength.

Fig. 7 (a) Electric-field dependence of recoverable energy-storage density and energy-storage efficiency of the PLZT AFE thick films with x = 0.08, 0.10, 0.12, and 0.14. The inset is the Weibull distribution and the fitting lines of breakdown strength of films. (b) Temperature dependence of energy-storage density and energy-storage efficiency these films measured at 900 kV/cm.

Fig. 8 The adiabatic temperature changes ΔT as a function of temperature under various applied electric field E of the PLZT AFE thick films with x = 0.08. The inset is polarization as a function

of temperature under different electric fields of the sample.

Fig. 9 The adiabatic temperature changes ΔT as a function of temperature under 990 kV/cm of the PLZT AFE thick films with x = 0.08, 0.10, 0.12, and 0.14.

Fig. 10 Different La content dependence of the temperature changes ΔT per electric field and the efficiency of refrigeration at 990 kV/cm.

Fig. 11 (a) Dielectric relaxation current of the PLZT AFE thick films with x = 0.08, 0.10, 0.12, and 0.14 under 400 kV/cm and room temperature. The inset is corresponding La content dependences of steady-state leakage current of the films. (b) Dielectric relaxation current of the thick films with x = 0.14 at different temperature. The inset gives the steady-state current density with the different temperature.

Fig. 1 Ye Zhao, *et.al.*

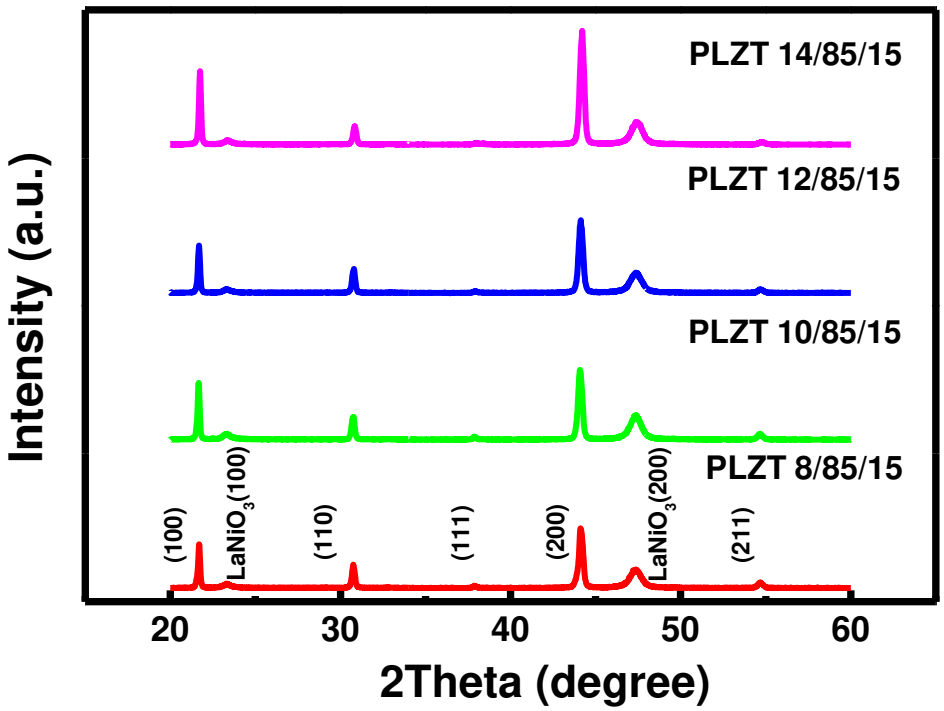

Fig. 2 Ye Zhao, *et.al.*

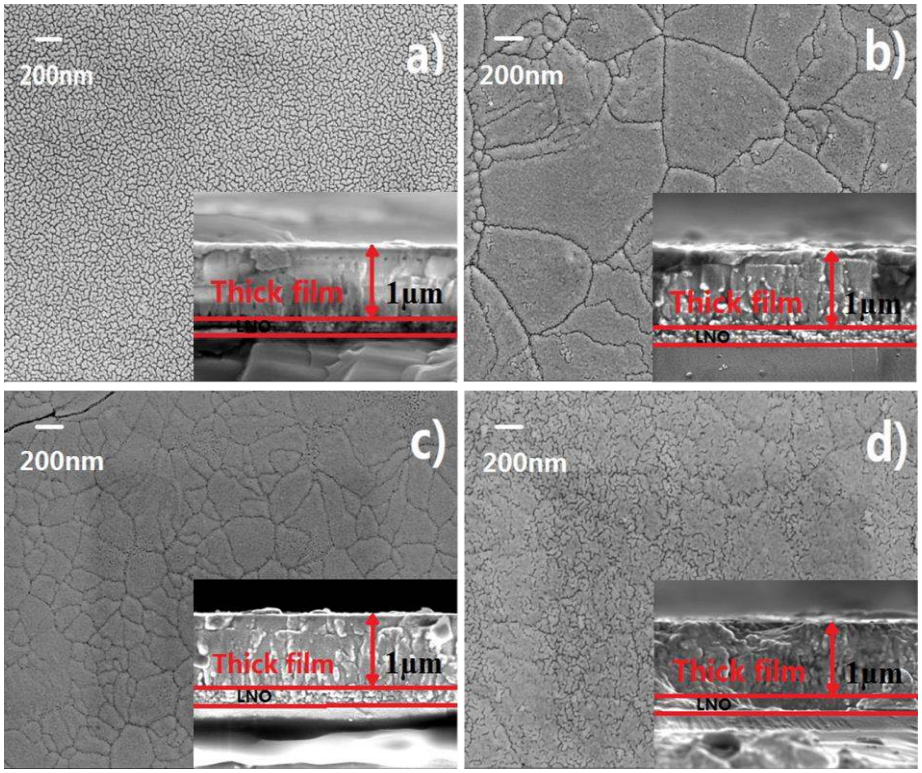

Fig. 3 Ye Zhao, *et.al.*

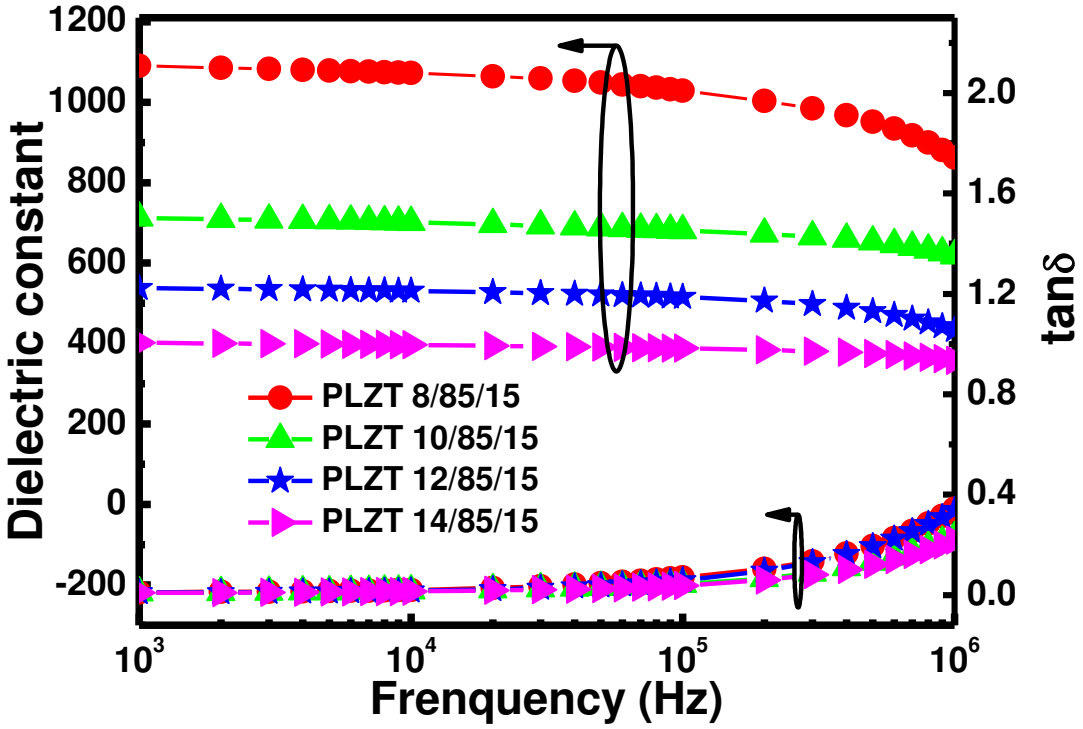

Fig. 4 Ye Zhao, *et.al.*

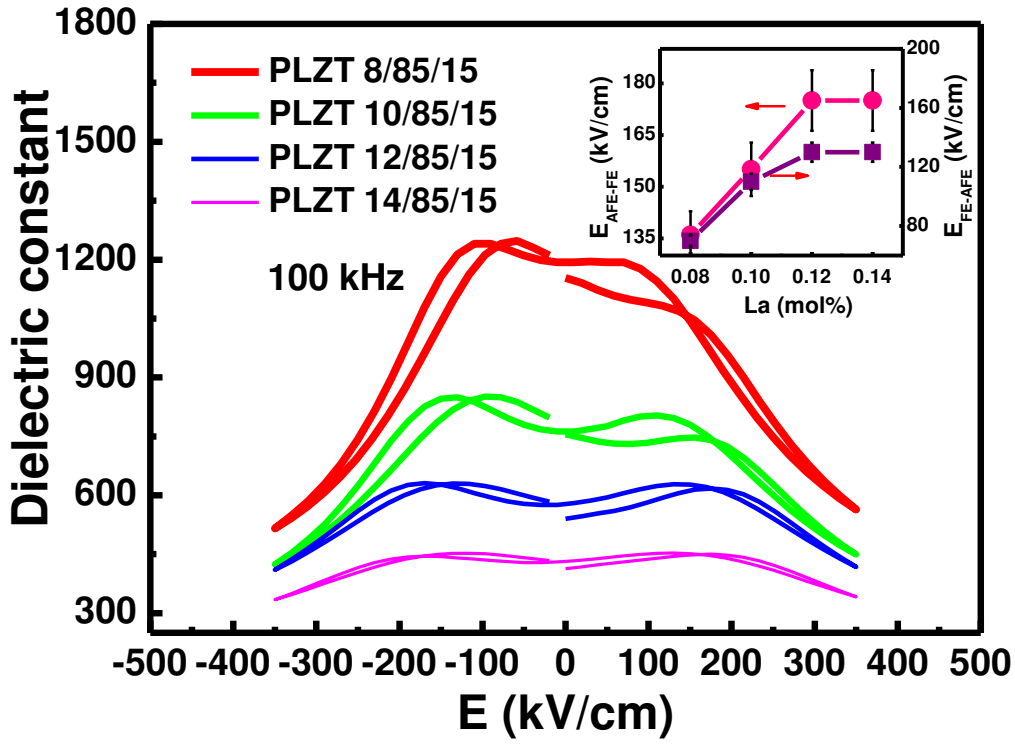

Fig. 5 Ye Zhao, *et.al.*

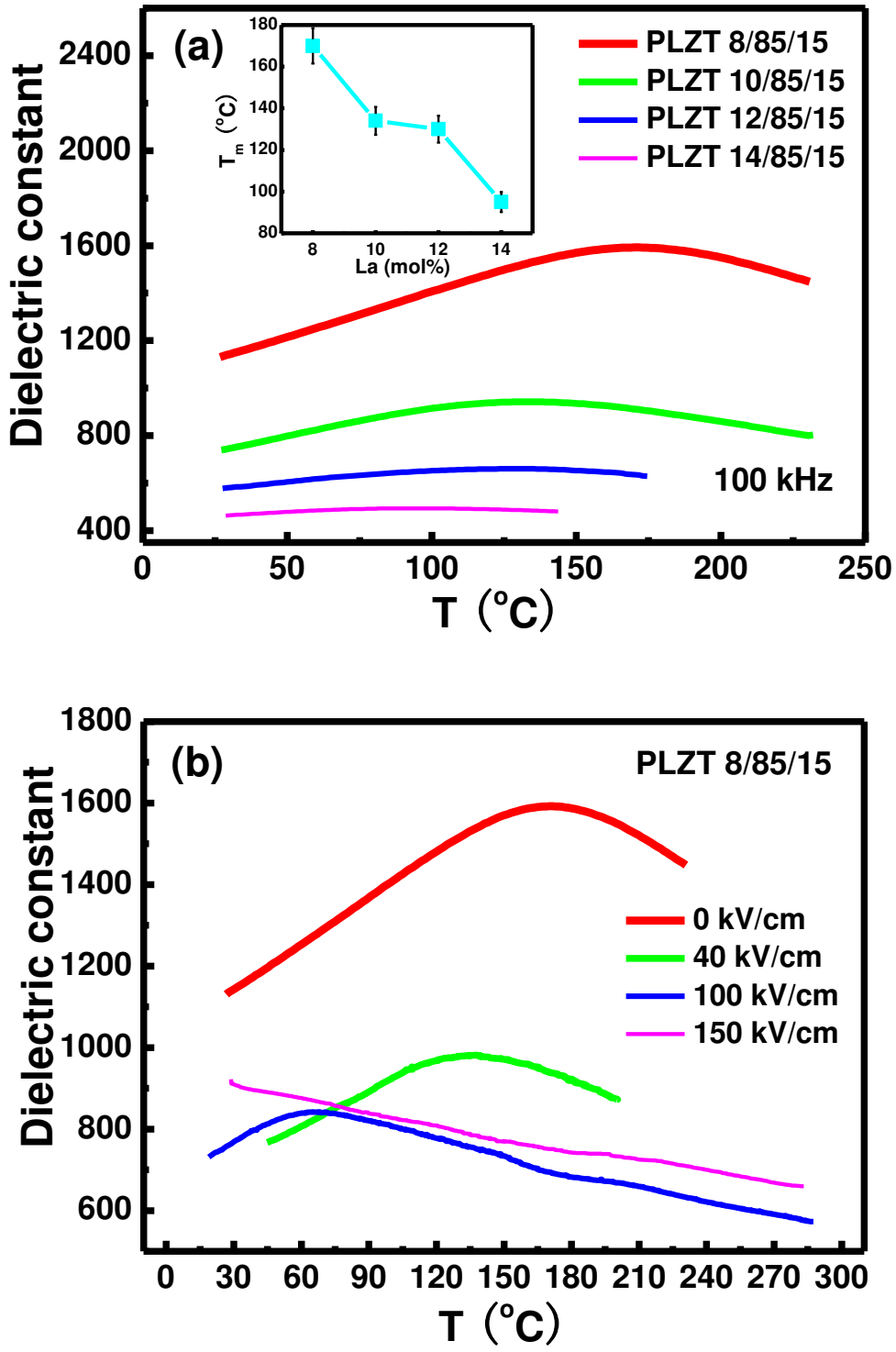

Fig. 6 Ye Zhao, *et.al.*

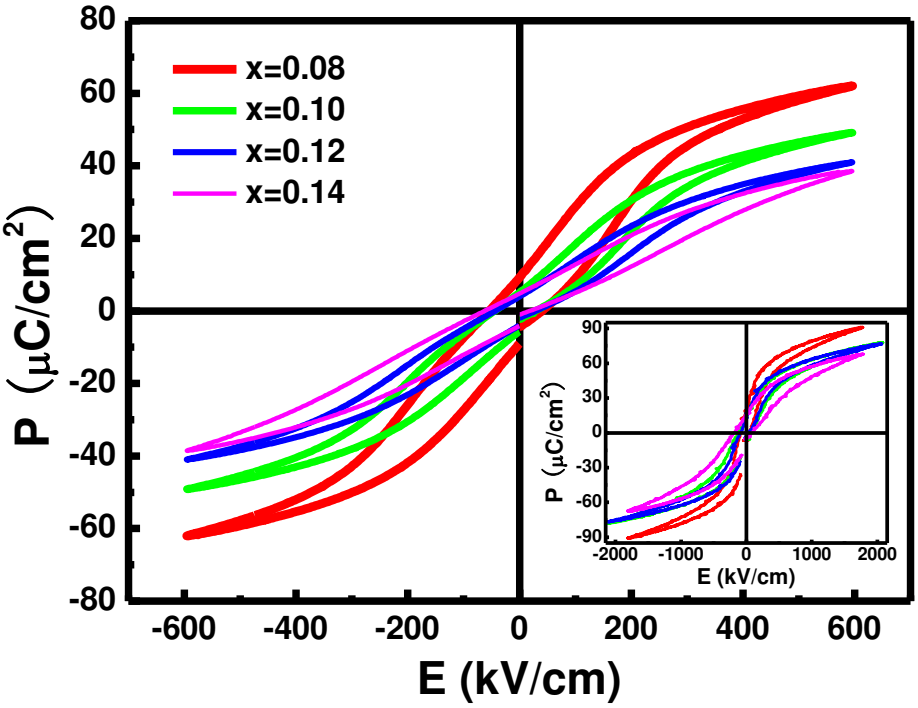

Fig. 7 Ye Zhao, *et.al.*

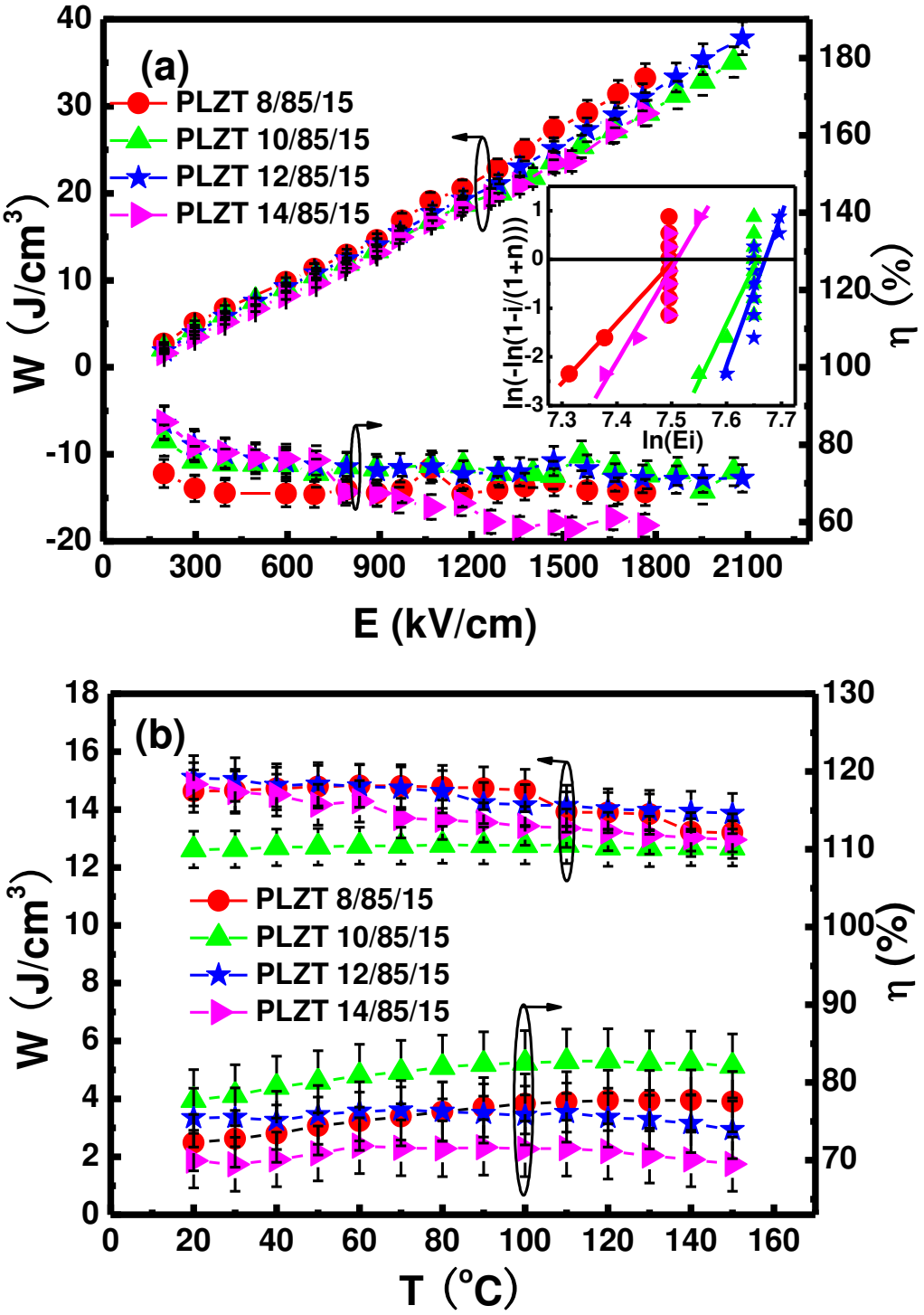

Fig. 8 Ye Zhao, *et.al.*

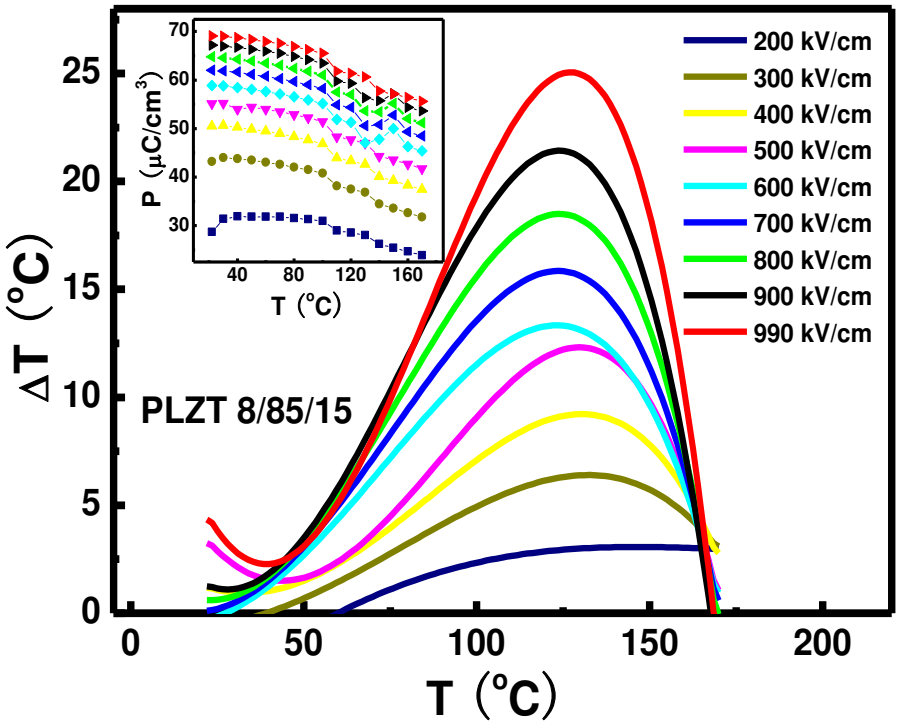

Fig. 9 Ye Zhao, *et.al.*

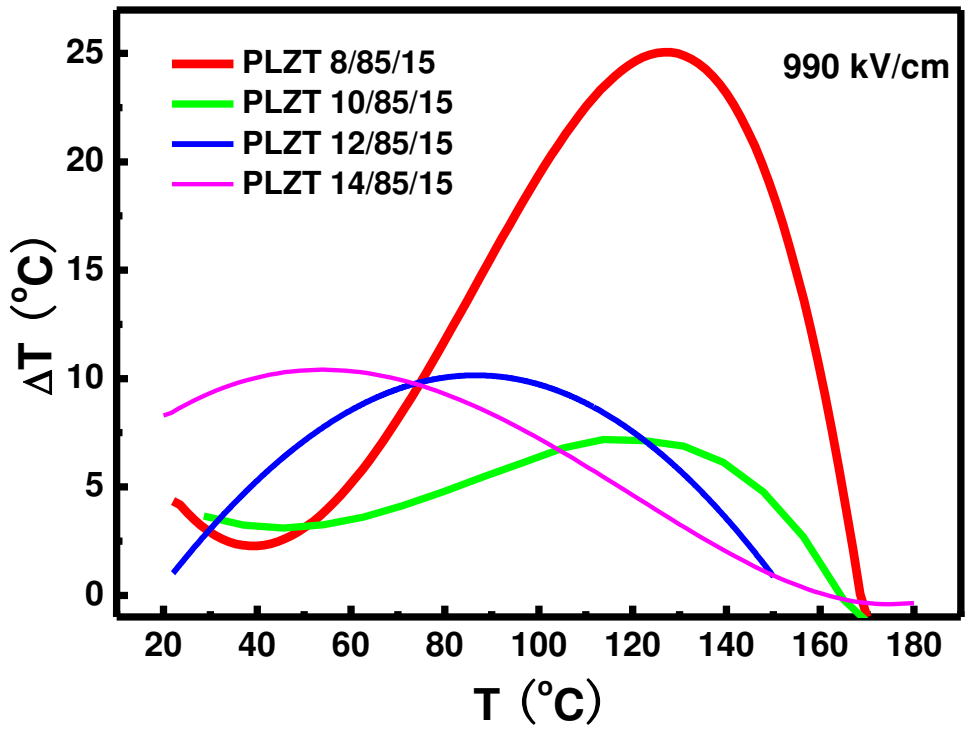

Fig. 10 Ye Zhao, *et.al.*

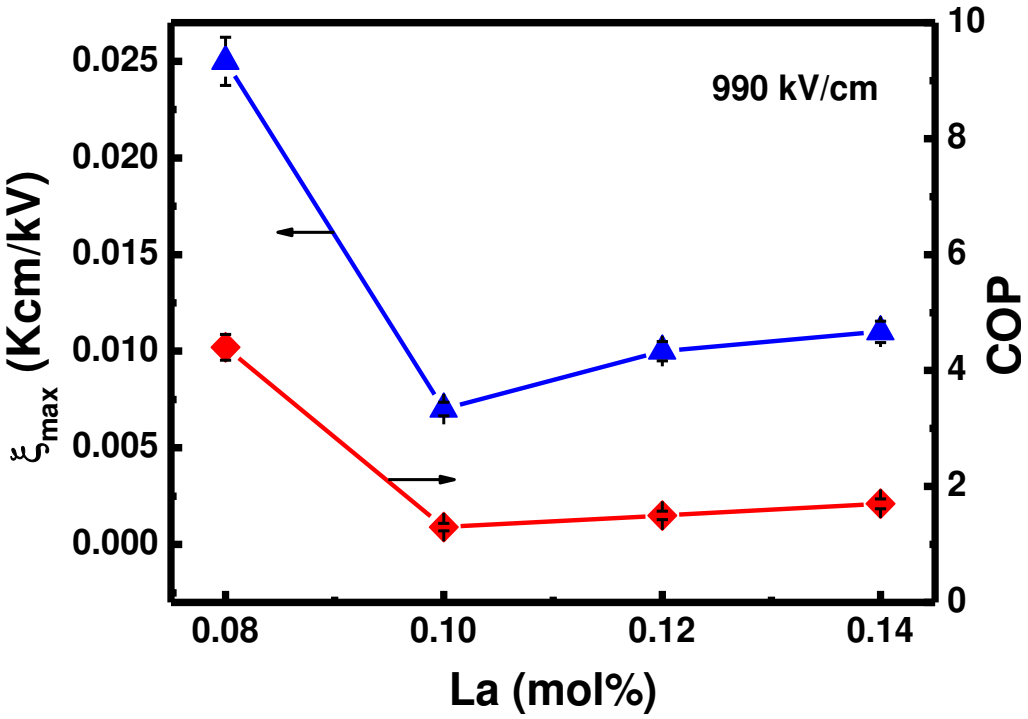

Fig. 11 Ye Zhao, *et.al.*

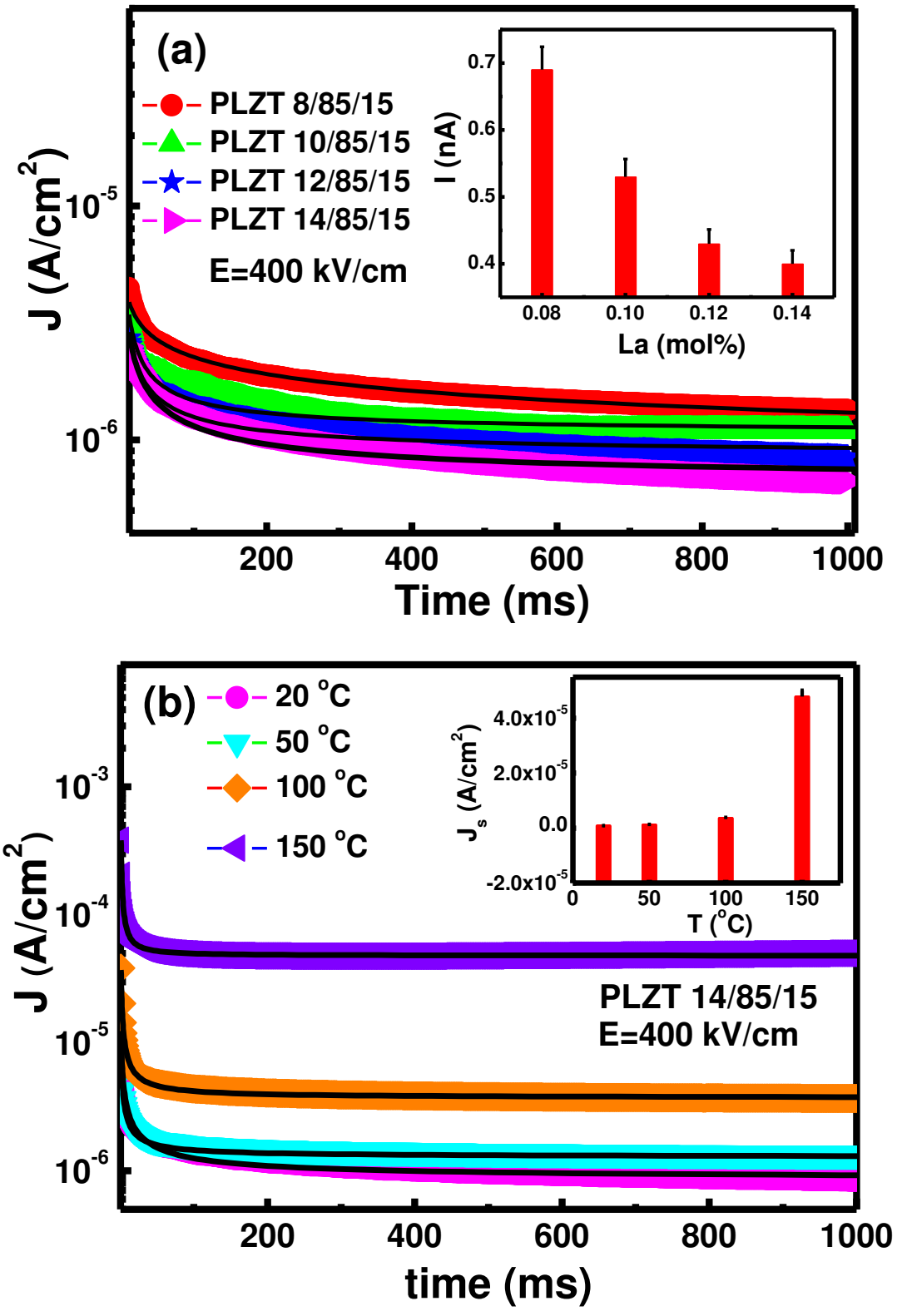

Table of Contents Graphic